Available online at www.sciencedirect.com
ScienceDirect
International Journal of Heat and Fluid Flow 28 (2007) 1244–1261
International Journal of HEAT AND FLUID FLOW
www.elsevier.com/locate/ijhff

Temporal large-eddy simulation of unstratified and stably stratified turbulent channel flows

Andrés E. Tejada-Martínez [a,*], Chester E. Grosch [b], Thomas B. Gatski [b,c]

[a] Department of Civil and Environmental Engineering, University of South Florida, Tampa, FL 33620, USA
[b] Department of Ocean, Earth and Atmospheric Sciences and Center for Coastal Physical Oceanography, Old Dominion University, Norfolk, VA 23529, USA
[c] Laboratoire d'Études Aérodynamiques, UMR CNRS 6609, Université de Poitiers, BP 30179, 86962 Futuroscope, Chasseneuil Cedex, France

Received 15 December 2006; received in revised form 4 June 2007; accepted 5 June 2007
Available online 1 August 2007

Abstract

Recently, Pruett et al. [Pruett, C.D., Gatski, T.B., Grosch, C.E., Thacker, W.D., 2003. The temporally filtered Navier–Stokes equations: properties of the residual stress. Phys. Fluids 15, 2127–2140] proposed an approach to large-eddy simulation (LES) based on time-domain filtering; their approach was termed temporal large-eddy simulation or TLES. In a continuation of their work, Pruett and collaborators tested their methodology by successfully performing TLES of unstratified turbulent channel flow up to Reynolds number of 590 (based on channel half-height and friction velocity) [Pruett, C.D., Thomas, B.C., Grosch, C.E., Gatski, T.B., 2006. A temporal approximate deconvolution model for LES. Phys. Fluids 18, 028104, 4p]. Here, we carefully analyze the TLES methodology in order to understand the role of its key components and in the process compare TLES to more traditional approaches of spatial LES. Furthermore, we extend the methodology to stably stratified turbulent channel flow.

Keywords: Turbulent flow; Temporal large-eddy simulation; Channel flow; Stratified flow

1. Introduction

In most common large-eddy simulation (LES) methodologies, a spatial filter is applied to the Navier–Stokes equations with the purpose of filtering out small turbulent scales, thereby allowing coarser discretizations to solve for the larger (resolved) turbulent scales governed by the filtered equations. Difficulties arise when extending spatial LES to unstructured grid-based methods, primarily related to commutation errors brought about by the spatial filtering of spatial differentiation operators. Well-characterized spatial filters on unstructured grids can be designed to minimize commutation errors, however, the computation of such filters can be algorithmically complex and can become expensive. A new approach which may potentially alleviate these shortcomings of spatial LES is based on time-domain filtering, recently introduced in Pruett et al. (2003, 2006), henceforth referred to as temporal LES or TLES. As noted by Pruett et al. (2006), TLES relies on the premise that the removal of high-frequency content from the frequency spectrum should effectively remove high-wavenumber content from the wavenumber spectrum as well, so that TLES can be performed at coarser temporal and spatial resolution than direct numerical simulation (DNS). This premise will be addressed below.

TLES is based on a splitting of the temporal scales into resolved filter-scale (RFS), resolved subfilter-scale (RSFS) and unresolved subfilter-scale (USFS) components. Note that this decomposition is the temporal counterpart of the spatial decomposition adopted in Yong et al. (2001) and later in Gullbrand and Chow (2003). The decomposition of the temporal scales into RFS, RSFS and USFS components leads to the temporally filtered Navier–Stokes equations (i.e. the TLES equations) governing the motions

* Corresponding author. Tel.: +1 757 617 2279.
E-mail address: tejada@ccpo.odu.edu (A.E. Tejada-Martínez).

0142-727X/$ - see front matter © 2007 Elsevier Inc. All rights reserved.
doi:10.1016/j.ijheatfluidflow.2007.06.002

of the RFS component. The TLES equations contain a subfilter-scale (SFS) stress, reflecting the effect of the RSFS and USFS components on the RFS component. The RSFS component of the SFS stress is approximated via temporal deconvolution while the USFS component is approximated via high order artificial viscosity in the form of a temporal regularization. Here, the effects of the (approximated) RSFS stress and the temporal regularization are analyzed in fully developed, unstratified turbulent channel flow. Furthermore, the TLES methodology is extended to fully developed, stably, thermally stratified turbulent channel flow.

2. Governing equations and TLES methodology

Application of a low-pass time-domain filter (see Pruett et al., 2003 and Pruett et al., 2006) to the non-dimensional, incompressible Navier–Stokes equations under the Boussinesq approximation yields the following time filtered equations:

$$\begin{aligned}
&\frac{\partial \bar{u}_i}{\partial x_i} = 0,\\
&\frac{\partial \bar{u}_i}{\partial t} + \frac{\partial \bar{u}_i \bar{u}_j}{\partial x_j} = -\frac{1}{\rho_0}\frac{\partial \bar{p}}{\partial x_i} + \frac{1}{Re_\tau}\frac{\partial^2 \bar{u}_i}{\partial x_j^2} + F\delta_{i1}\\
&\qquad\qquad - Ri_\tau(\bar{\rho} - \bar{\rho}_\mathrm{b})\delta_{i3} - \frac{\partial \tau_{ij}}{\partial x_j},\\
&\frac{\partial \bar{\rho}}{\partial t} + \frac{\partial \bar{\rho}\bar{u}_j}{\partial x_j} = \frac{1}{Re_\tau Pr}\frac{\partial^2 \bar{\rho}}{\partial x_j^2} - \frac{\partial \lambda_j}{\partial x_j}.
\end{aligned} \tag{1}$$

In (1), an over-bar denotes application of the time-domain filter, $\bar{u}_i$ is the i-component of the time filtered velocity field, $\bar{p}$ is the filtered pressure, and $\bar{\rho}$ is the filtered perturbation density. In obtaining the equations in (1) the filtered total density $\bar{\rho}^*$ has been decomposed as

$$\bar{\rho}^*(x_1, x_2, x_3, t) = \rho_0 + \bar{\rho}(x_1, x_2, x_3, t), \tag{2}$$

where $\bar{\rho} \ll \rho_0$. The filtered perturbation density has been further decomposed as

$$\bar{\rho}(x_1, x_2, x_3, t) = \bar{\rho}_\mathrm{b}(x_3, t) + \bar{\rho}'(x_1, x_2, x_3, t), \tag{3}$$

where $\bar{\rho}_\mathrm{b}$ is the instantaneous, spatial mean density profile and $\bar{\rho}'$ is its fluctuating component. Due to the previous decompositions, the filtered pressure $\bar{p}$ in (1) is the pressure which remains after the component that is in hydrostatic balance with the bulk density field is removed. In the case of the turbulent channel flows considered here, $\bar{\rho}_\mathrm{b}$ is obtained by averaging $\bar{\rho}$ over (x_1, x_2)-planes parallel to the channel walls. Term F, appearing in the x_1-momentum equation in (1), is an imposed non-dimensional mean pressure gradient driving the flows in the x_1-direction. F is unity as the equations in (1) have been made non-dimensional with the friction velocity u_τ and channel half-height h. The non-dimensional parameters are as follows: $Re_\tau = u_\tau h/\nu$ is the Reynolds number with ν the kinematic viscosity, and $Ri_\tau = \Delta\rho g h/\rho_0 u_\tau^2$ is the Richardson number with g gravity and $\Delta\rho$ the difference between $\bar{\rho}$ at the top and bottom walls. Molecular diffusivity is denoted by κ where $\kappa = \nu/Pr$ with Pr the Prandtl number. In our simulations, $Pr = 0.71$, corresponding to thermally stratified air. The previous formulation of the governing equations is the same as that in Armenio and Sarkar (2002).

The filtering operation gives rise to a closure problem in the form of the SFS stress and the SFS density flux,

$$\tau_{ij} = \overline{u_i u_j} - \bar{u}_i \bar{u}_j \tag{4}$$

and

$$\lambda_j = \overline{\rho u_j} - \bar{\rho}\bar{u}_j, \tag{5}$$

respectively. The SFS stress and SFS density flux are unknown because the unfiltered velocity, u_i, and the unfiltered perturbation density, ρ, are not accessible in LES. Thus, the SFS stress and SFS density flux must be modeled and/or approximated. Conceptually, the full (unfiltered) velocity may be expressed as

$$u_i = \bar{u}_i + u_i^{\mathrm{SFS}}, \tag{6}$$

where $\bar{u}_i$ and u_i^{SFS} are the resolved filter-scale (RFS) (i.e. the filtered velocity) and the subfilter-scale (SFS) components, respectively. The width of the low-pass time filter used to obtain the filtered equations in (1) is greater than the time step of the temporal numerical discretization of (1). Thus, the temporal discretization can resolve higher frequencies than those permitted by the low-pass time filter leading to the following decomposition of the SFS velocity:

$$u_i^{\mathrm{SFS}} = u_i^{\mathrm{RSFS}} + u_i^{\mathrm{USFS}}, \tag{7}$$

where u_i^{RSFS} and u_i^{USFS} are the resolved subfilter-scale (RSFS) and unresolved subfilter-scale (USFS) components, respectively. To help better understand this decomposition, Fig. 1 shows a sketch of the range of frequencies spanned by these components.

Following the TLES methodology and inserting (7) in (6) leads to

$$u_i = \underbrace{\bar{u}_i + u_i^{\mathrm{RSFS}}}_{=v_i} + u_i^{\mathrm{USFS}} \tag{8}$$

where v_i is an approximately deconvolved or defiltered velocity obtained by applying an approximate inverse of the time filter to $\bar{u}_i$; this procedure is explained in detail

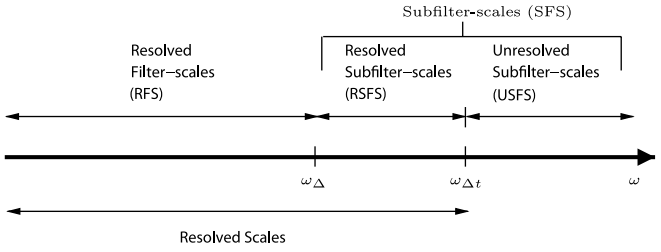

Fig. 1. Sketch of the range of frequencies, ω, spanned by velocity scales relevant to TLES. ω_Δ is the highest frequency permitted by the low-pass time filter. ω_Δ is inversely proportional to Δ, the width of the time filter. $\omega_{\Delta t}$ is the highest frequency resolved by the discretization. $\omega_{\Delta t}$ is inversely proportional to Δt, the time step used by the discretization.

in Pruett et al. (2006). Note that the frequency content of v_i is as high as that permitted by the temporal discretization. Furthermore, the frequency content of $\bar{u}_i$ is as high as that permitted by the time filter. The highest frequency content in $\bar{u}_i$ is lower than the highest frequency content permitted by the discretization and thus the highest frequency content in v_i as well. Inserting the decomposition in (8) into (4) leads to

$$\tau_{ij} = \underbrace{\overline{v_i v_j} - \bar{v}_i \bar{v}_j}_{\text{approximate RSFS stress, } \tau_{ij}^{\text{RSFS}}} + \text{USFS stress}. \tag{9}$$

A similar decomposition allows re-expression of (5) as

$$\lambda_j = \underbrace{\overline{\varrho v_j} - \bar{\varrho}\bar{v}_j}_{\text{approximate RSFS density flux, } \lambda_j^{\text{RSFS}}} + \text{USFS density flux}, \tag{10}$$

where ϱ is an approximately deconvolved density. The approximate deconvolution procedure (based on the van Cittert method and explained in detail in Pruett et al. (2006)) leads to

$$v_i = C_0\bar{u}_i + C_1\bar{\bar{u}}_i + C_2\bar{\bar{\bar{u}}}_i + C_3\bar{\bar{\bar{\bar{u}}}}_i. \tag{11}$$

where the series has been truncated at four terms following the work of Pruett et al. (2006). Effects of including additional or fewer terms should be pursued in the future. For our extension to stably stratified flows, we propose a similar expression for ϱ, that is

$$\varrho = C_0\bar{\rho} + C_1\bar{\bar{\rho}} + C_2\bar{\bar{\bar{\rho}}} + C_3\bar{\bar{\bar{\bar{\rho}}}}. \tag{12}$$

The coefficients $[C_0, C_1, C_2, C_3] = [0, \sqrt{6}, \sqrt{4+2\sqrt{6}} - 2\sqrt{6}, 1 - \sqrt{4+2\sqrt{6}} + \sqrt{6}]$ are derived in Pruett et al. (2006) with the aim of minimizing phase error effects associated with temporal filters. Note that the deconvolution series in (11) and (12) extends up to four terms.

An analogous spatial decomposition to the temporal decomposition in (8) together with a lowest order approximation of v_i as $v_i \sim \bar{u}_i$ and subsequent insertion into the residual or subfilter-scale stress leads to what are traditionally referred to as the Leonard stress, the cross-stress, and the subgrid-scale (SGS) Reynolds stress (Pope, 2000). The Leonard stress is expressed in terms of the resolved velocity, thus this stress is often referred to as the resolved Leonard stress and corresponds to the approximate RSFS stress in (9). The Leonard stress is also often referred to as the scale similarity stress. Stolz and Adams (1999), who introduced the approximate deconvolution method for spatial LES, refer to their spatial counterpart of the approximate RSFS stress in (9) as a generalized scale similarity stress given that in general $v_i \neq \bar{u}_i$. Finally, the cross-stress and the SGS Reynolds stress are expressed in terms of the unresolved velocity component and form what we would refer to as the USFS stress.

The negative of the divergence of the USFS stress appearing on the right hand side (r.h.s.) of the second equation in (1) (via (9)) is modeled by a temporal regularization term expressed as $-\chi_1(\bar{u}_i - \bar{w}_i)$, where w_i is a second deconvolved velocity. In essence, this term behaves as a high order artificial viscosity. The approximately deconvolved velocity, w_i, is computed in the same form as in (11) with coefficients $[C_0, C_1, C_2, C_3] = [15/8, -9/8, 1/4, 0]$, as derived in Pruett et al. (2006) by imposing that the regularization term is strictly of dissipative nature. Similarly, we propose that the negative of the divergence of the USFS density flux (appearing on the r.h.s. of the third equation in (1) via (10)) be replaced by $-\chi_2(\bar{\rho} - \bar{\vartheta})$, where ϑ is obtained just as ϱ in (12) with the same coefficients used to obtain w_i. Constant coefficients χ_1 and χ_2 are arbitrary and were taken as $\chi_1 = \chi_2 = 1$ in our simulations, following (Pruett et al., 2006). Future simulations will address dependence of results on these parameters. In summary, the equations we solve numerically are given as follows:

$$\begin{aligned}
&\frac{\partial \bar{u}_i}{\partial x_i} = 0,\\
&\frac{\partial \bar{u}_i}{\partial t} + \frac{\partial \bar{u}_i\bar{u}_j}{\partial x_j} = -\frac{1}{\rho_0}\frac{\partial \bar{p}}{\partial x_i} + \frac{1}{Re_\tau}\frac{\partial^2 \bar{u}_i}{\partial x_j^2} + F\delta_{i1} - Ri_\tau(\bar{\rho} - \bar{\rho}_b)\delta_{i3}\\
&\qquad\qquad - \frac{\partial \tau_{ij}^{\text{RSFS}}}{\partial x_j} - \chi_1(\bar{u}_i - \bar{w}_i),\\
&\frac{\partial \bar{\rho}}{\partial t} + \frac{\partial \bar{\rho}\bar{u}_j}{\partial x_j} = \frac{1}{Re_\tau Pr}\frac{\partial^2 \bar{\rho}}{\partial x_j^2} - \frac{\partial \lambda_j^{\text{RSFS}}}{\partial x_j} - \chi_2(\bar{\rho} - \bar{\vartheta}).
\end{aligned} \tag{13}$$

In Pruett et al. (2006), the TLES methodology previously described was shown feasible on unstratified turbulent channel flows without the scalar equation for $\bar{\rho}$ in (13). In addition to extending TLES to stably stratified flows and thus the scalar equation in (13), a major goal of our studies is to isolate and understand the effects of the resolved subfilter scales (ie. τ_{ij}^{RSFS} and λ_j^{RSFS}) and regularization on simulation results.

3. Numerical method

The numerical method solving the governing equations employed a hybrid pseudo-spectral/finite-difference discretization. Streamwise and spanwise directions (x_1 and x_2) were discretized spectrally via Fourier series and the vertical direction (x_3) was discretized via high order (fifth and sixth order) compact finite-difference schemes, allowing grid stretching. Time-marching consisted of the second order time-accurate pressure correction scheme on a non-staggered grid analyzed in Armfield and Street (2000) and Fringer et al. (2003). In order to prevent spurious accumulation of energy at the highest resolvable wavenumbers brought about by nonlinear terms, we perform de-aliasing using the well-known 3/2-rule in the horizontal directions. In the vertical direction, we use a high order filter in order to attenuate the spurious high-wavenumber energy accumulation while fully preserving the more energetic scales at lower wavenumber. Details of the method can be found in Tejada-Martínez and Grosch (2006).

4. Unstratified turbulent channel flow

We present results from TLES of fully developed, unstratified (i.e. $Ri_\tau = 0$) turbulent channel flow between two parallel plates or walls driven by a mean pressure gradient (as described in Section 2) such that $Re_\tau = 180$. Following the DNS in Kim et al. (1987), the computational domain was chosen $L_1 = 4\pi h$ long in the streamwise (x_1) direction, $L_2 = 4\pi h/3$ wide in the spanwise (x_2) direction, and $2h$ high in the vertical (x_3), wall-normal direction. The domain extended from $x_3 = -h$ to $x_3 = h$ in the vertical. No-slip velocity and fixed perturbation densities were imposed at the walls and periodicity was prescribed in x_1 and x_2.

Prior to performing TLES, the code implementing the numerical method was validated via spatial LES and DNS of the previously described problem. In the spatial LES, the SFS stress was not decomposed into resolved and unresolved (i.e. RSFS and USFS) components in order to model or approximate each component separately, as in TLES. Instead, the entire SFS stress was modeled via the dynamic Smagorinsky model (or simply dynamic model):

$$\tau_{ij}^{\mathrm{SFS(d)}} \equiv \left(\tau_{ij}^{\mathrm{SFS}} - \frac{1}{3}\tau_{kk}^{\mathrm{SFS}}\delta_{ij}\right) = -2(C_s\overline{\Delta})^2|\overline{S}|\overline{S}_{ij}, \tag{14}$$

where the strain rate tensor is $\overline{S}_{ij} = (\bar{u}_{i,j} + \bar{u}_{j,i})/2$ and $|\overline{S}| = (2S_{ij}S_{ij})^{1/2}$ is its norm. The isotropic part of the SFS stress, $\frac{1}{3}\tau_{kk}^{\mathrm{SFS}}\delta_{ij}$ is added to the pressure. The model coefficient, $(C_s\overline{\Delta})^2$, is obtained dynamically via the modified Germano dynamic procedure proposed in Lilly (1992). The test filtering required for the dynamic procedure was performed over x_1 and x_2 with a box filter of width $2\Delta x_1$ in x_1 and $2\Delta x_2$ in x_2, where Δx_1 and Δx_2 are the constant grid cell sizes in x_1 and x_2, respectively. The box filter was approximated with the trapezoidal rule, leading to a test filter width of $\sqrt{6}\Delta x_i$, as computed in Lund (1997). Thus, the dynamic model parameter (i.e. the filter width ratio) was set to $\sqrt{6}$. The computational grid consisted of 32 modes in x_1, 32 modes in x_2 and 65 points in x_3 (i.e. $(32\times32\times65)$). In the DNS, the grid was $(96\times96\times97)$. In both, the spatial LES and the DNS, a hyperbolic tangent function was used in the x_3 direction to cluster more points near the top and bottom walls in order to resolve sharper gradients in these regions. Furthermore, the first (x_1, x_2)-plane of grid points away from the bottom (*viz.* top) wall was at a distance $\Delta x_3^+ = \Delta x_3 u_\tau/\nu = 1$, within the viscous sublayer. In the spatial LES, the time step was $\Delta t = 0.005$ and in the DNS, $\Delta t = 0.001$, for temporal accuracy.

In terms of mean velocity, resolved Reynolds stress components, and one-dimensional spectra (not shown), spatial LES performed with our method was more accurate than spatial LES performed with lower order discretization methods, as expected. DNS with our method also performed well as results were nearly indistinguishable from the DNS results of Kim et al. (1987). The latter DNS was performed on a $(128\times128\times129)$ grid.

All TLES cases presented were performed on the same grid with the same time step as the previously described

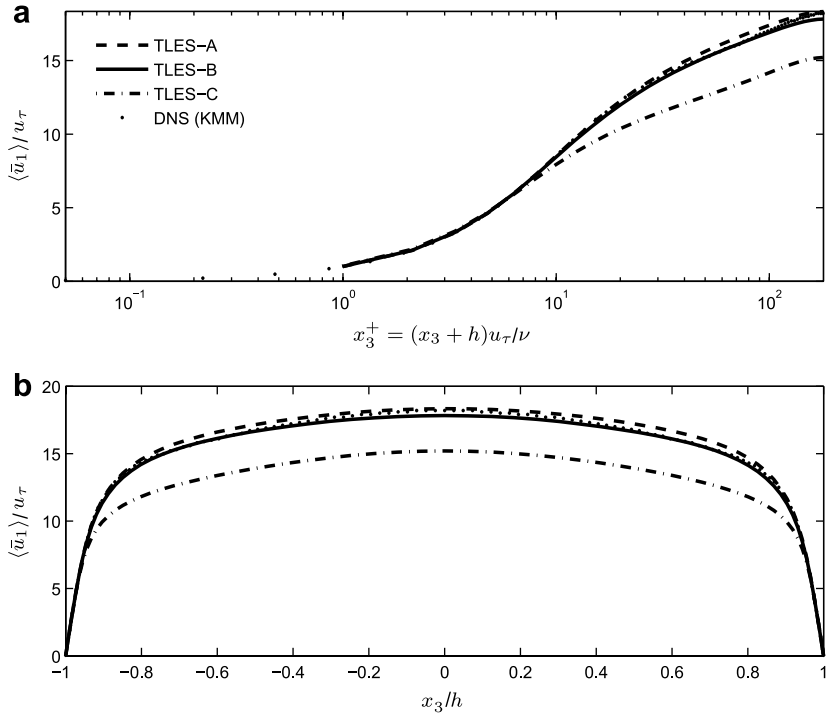

Fig. 2. Mean streamwise resolved velocity in (a) wall units and (b) units of h in TLES of unstratified flows. Angle brackets denote averaging in time and over (x_1, x_2)-planes. TLES-A: TLES with regularization of momentum only; TLES-B: TLES with both regularization of momentum and RSFS stress; TLES-C: TLES with RSFS stress only; DNS (KMM): direct numerical simulation of Kim, Moin and Moser in Kim et al. (1987). Note that the DNS result is nearly indistinguishable from the TLES-B result except in the core region ($x_3 \sim 0$).

spatial LES. The width of the time filter was taken as $\Delta = 64\Delta t$, thus $\Delta = 0.32$ (i.e. $64 \cdot 0.005 = 0.32$), which was the same value used in Pruett et al. (2006).

4.1. Effect of regularization and RSFS stress on momentum transport

In order to understand the effect of regularization and RSFS stress on momentum transport, we employ a comparison strategy similar to that adopted by Morinishi and Vasilyev (2001) to explain differences between the dynamic mixed model, the dynamic Smagorinsky model and the scale similarity approximation. In Figs. 2, 4, and 6, we plot TLES results from three simulations, one simulation with only regularization and no RSFS stress, a second with regularization and RSFS stress, and a third with only RSFS stress and no regularization. In Fig. 2, we see that using the RSFS stress by itself leads to a severe under-prediction of the mean x_1 velocity. Using regularization by itself leads to a slight over-prediction of the mean velocity. Using regularization together with the RSFS stress leads to a better estimate. As can be seen by comparing Figs. 2 and 3, the previous results are analogous to results of spatial LES with the dynamic Smagorinsky model, the dynamic mixed model and the scale similarity approximation. More specifically, the result of TLES with only RSFS stress is analogous to that of spatial LES with the scale similarity approximation, the result of TLES with regularization is analogous to that of spatial LES with only regularization, and the result of TLES with both regularization and RSFS stress is analogous to that of spatial LES with the dynamic mixed model. In these spatial LES approaches, the SFS stress is not split into RSFS and USFS components; instead, the SFS stress is either modeled or approximated. For example, in the case of the scale similarity approximation in Bardina et al. (1983) (often referred to as the Bardina model), the deviatoric component of the SFS stress is approximated as

$$\tau_{ij}^{\mathrm{SFS(d)}} \equiv \left(\tau_{ij}^{\mathrm{SFS}} - \frac{1}{3}\tau_{kk}^{\mathrm{SFS}}\delta_{ij}\right) \approx \left(\overline{\bar{u}_i\bar{u}_j} - \bar{\bar{u}}_i\bar{\bar{u}}_j\right)^d \tag{15}$$

where now the over-bar notation denotes application of a homogeneous spatial filter. Just as with the dynamic Smagorinsky model, the deviatoric component of $\tau_{ij}^{\mathrm{SFS(d)}}$ is approximated while its isotropic component is added to the pressure. Numerous researchers (e.g. Morinishi and Vasilyev in Morinishi and Vasilyev (2001)) have shown that this approximation results in an SFS stress lacking sufficient turbulent kinetic energy dissipation. However, the resulting stress is merited by its strong correlation with the exact SFS stress (for example, see Horiuti, 1989). As a way to alleviate the lack of turbulent kinetic energy dissipation of the scale similarity approximation while still retaining its merit of possessing a strong correlation with the exact SFS stress, researchers have proposed the dynamic mixed model (see for example Zang et al., 1993) in which the SFS stress is given in terms of a scale similarity component and a Smagorinsky component. In a variant of this approach (see Salvetti and Banerjee, 1994), the SFS stress is given as:

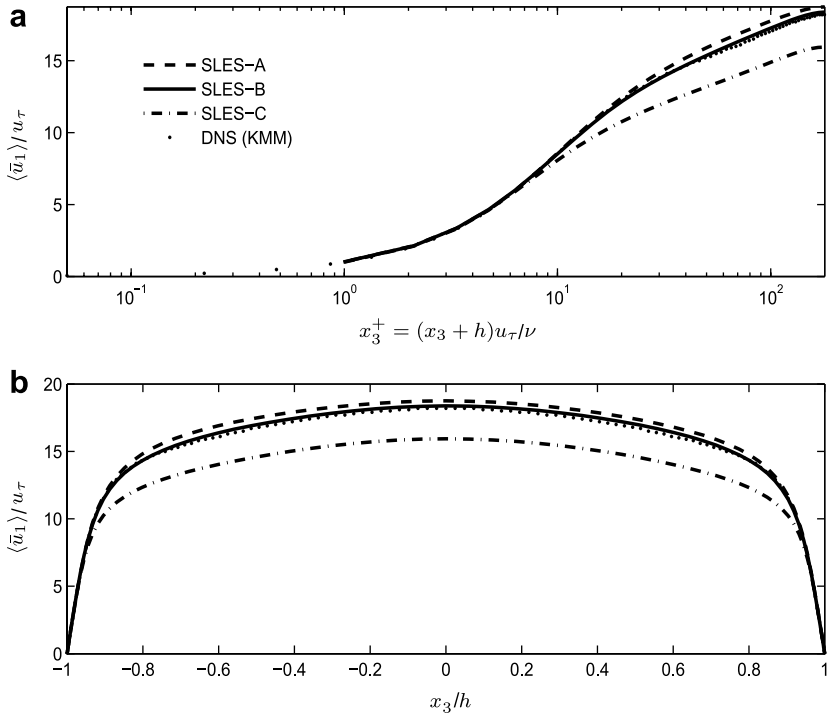

Fig. 3. Mean streamwise resolved velocity in (a) wall units and (b) units of h in spatial LES of unstratified flows. SLES-A: spatial LES with dynamic Smagorinsky model; SLES-B: spatial LES with dynamic mixed model; SLES-C: spatial LES with scale similarity approximation; DNS (KMM): direct numerical simulation of Kim, Moin and Moser in Kim et al. (1987). Note that the DNS result is very close to the SLES-B result.

$$\tau_{ij}^{\mathrm{SFS(d)}} = C_{\mathrm{L}}(\overline{\bar{u}_i\bar{u}_j} - \bar{\bar{u}}_i\bar{\bar{u}}_j)^d - 2(C_{\mathrm{s}}\overline{\Delta})^2|\overline{S}|\overline{S}_{ij}, \tag{16}$$

where the model coefficients C_{L} and $(C_{\mathrm{s}}\overline{\Delta})^2$ are determined dynamically. Note that in Zang et al. (1993), $C_{\mathrm{L}} = 1$ and $(C_{\mathrm{s}}\overline{\Delta})^2$ is determined dynamically. In our implementation, $(C_{\mathrm{s}}\overline{\Delta})^2$ and C_{L} are determined dynamically using the modified procedure proposed by Morinishi and Vasilyev (2001).

In (16), the filter denoted with an over-bar is required for obtaining the $\overline{\bar{u}_i\bar{u}_j}$ and $\bar{u}_i\bar{u}_j$ terms. Note that the scale similarity approximation as well as the dynamic mixed model require use of the homogeneous spatial filter denoted with an over-bar. In practice this filter is not well-defined as it is depends on an unknown combination of the subfilter-scale model, the discretization, and the grid size. In our implementation we have used the filter in equation (21) of Morinishi and Vasilyev (2001),

$$\bar{f}(x) = \frac{1}{24}[f(x-h) + 22f(x) + f(x+h)], \tag{17}$$

in both x_1 and x_2 directions where h (the filter width) is the grid spacing in x_1 or x_2. Furthermore, the test filtering operation required in the modified dynamic procedure is the same one used for the dynamic Smagorinsky model described earlier.

Next, we look at TLES results in terms of resolved Reynolds stress $\langle\bar{u}_i'\bar{u}_j'\rangle \equiv \langle\bar{u}_i\bar{u}_j\rangle - \langle\bar{u}_i\rangle\langle\bar{u}_j\rangle$, effective resolved Reynolds stress, $\langle\bar{u}_i'\bar{u}_j' + \tau_{ij}^{\mathrm{RSFS}}\rangle$, and root mean square of resolved velocity fluctuations, $\bar{u}_i^{\mathrm{rms}} \equiv \langle\bar{u}_i'\bar{u}_i'\rangle^{1/2}$. In this last expression, the repeated index does not imply summation. Angle brackets denote averaging in time and over (x_1,x_2)-planes. These definitions are based on the classical Reynolds decomposition, which for LES can be expressed as $\bar{u}_i = \langle\bar{u}_i\rangle + \bar{u}_i'$. Note that in TLES with only regularization, the effective resolved Reynolds stress is equivalent to the resolved Reynolds stress because $\tau_{ij}^{\mathrm{RSFS}} = 0$.

In Fig. 4 we see that TLES with only RSFS stress greatly over-predicts the 1–3 component of the Reynolds shear stress as the peak of the effective resolved Reynolds shear stress is much greater than the peak of the DNS result. Predictions by TLES with only regularization and TLES with regularization and RSFS stress are both excellent.

Notice that the contribution of the 1–3 RSFS stress ($\tau_{13}^{\mathrm{RSFS}}$) to the effective 1–3 resolved Reynolds stress, in the TLES with regularization and RSFS stress, is substantial. Thus, inclusion of $\tau_{13}^{\mathrm{RSFS}}$ for prediction of 1–3 Reynolds shear stress is crucial. These results are analogous to results with the various spatial LES models in the same fashion discussed earlier, as can be seen by comparing Figs. 4 and 5.

The root mean square of resolved velocity fluctuations (i.e. $\bar{u}_i^{\mathrm{rms}}$) obtained in our three variations of TLES are plotted in Fig. 6 and are compared with DNS-predicted values. Note that the DNS results are not based on filtered velocity fields, which would lead to lower values of $\bar{u}_i^{\mathrm{rms}}$. Thus, it would be desirable that, for example, the peak values of $\bar{u}_i^{\mathrm{rms}}$ predicted by TLES are less than the peaks of the DNS. TLES with only regularization over-predicts the

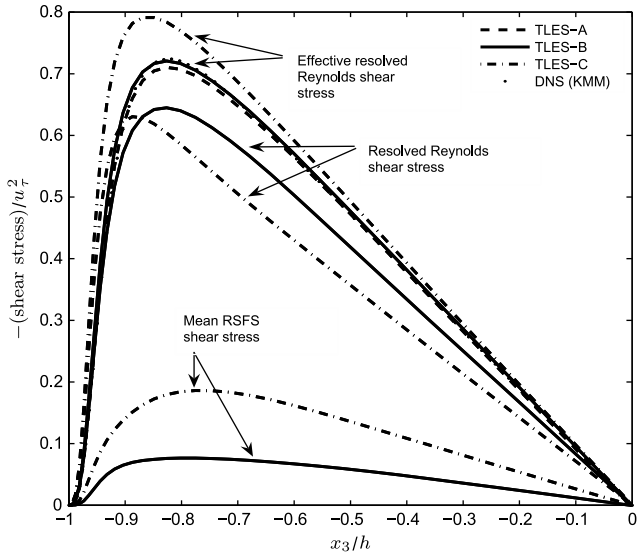

Fig. 4. One to three components of resolved Reynolds shear stress, $\langle\bar{u}_1'\bar{u}_3'\rangle$, mean RSFS shear stress, $\langle\tau_{13}^{\mathrm{RSFS}}\rangle$, and effective resolved Reynolds shear stress, $\langle\bar{u}_1'\bar{u}_3'\rangle + \langle\tau_{13}^{\mathrm{RSFS}}\rangle$ of unstratified flows. TLES-A: TLES with regularization of momentum only; TLES-B: TLES with both regularization of momentum and RSFS stress; TLES-C: TLES with RSFS stress only; DNS (KMM): direct numerical simulation of Kim, Moin and Moser in Kim et al. (1987). Note that the DNS result is nearly indistinguishable from the TLES-B result.

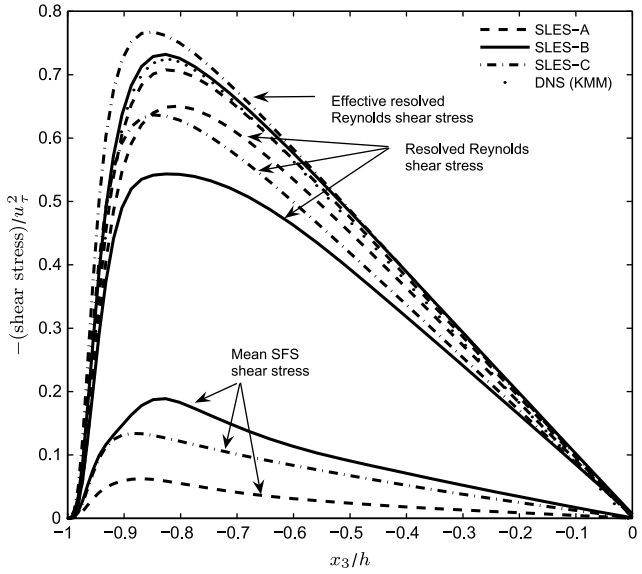

Fig. 5. One to three components of resolved Reynolds shear stress, effective resolved Reynolds shear stress and mean RSFS shear stress in spatial LES of unstratified flows. SLES-A: spatial LES with dynamic Smagorinsky model; SLES-B: spatial LES with dynamic mixed model; SLES-C: spatial LES with scale similarity approximation; DNS (KMM): direct numerical simulation of Kim, Moin and Moser in Kim et al. (1987).

expected value of $\bar{u}_1^{\mathrm{rms}}$. TLES with regularization and RSFS stress also over-predicts this value, however, its predicted value is lower than that of the TLES with only regularization. The peak value in TLES with only RSFS stress is lower than in the other two variations of TLES. The ordering

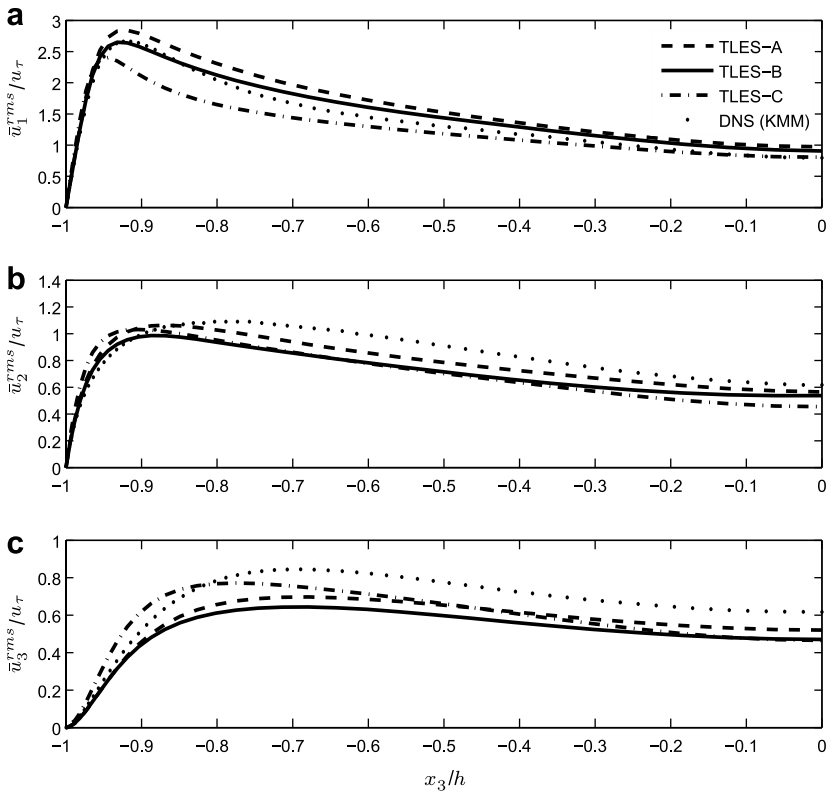

Fig. 6. Root mean square of resolved velocity fluctuations in TLES of unstratified flows. TLES-A: TLES with regularization of momentum only; TLES-B: TLES with both regularization of momentum and RSFS stress; TLES-C: TLES with RSFS stress only; DNS (KMM): direct numerical simulation of Kim, Moin and Moser in Kim et al. (1987).

of the peak values of $\bar{u}_1^{\text{rms}}$ in the TLES cases is analogous to the ordering of the peak values in the spatial LES cases, as can be seen by comparing Figs. 6 and 7. Based on this ordering and as noted earlier, results in the TLES with only regularization are analogous to those in spatial LES with the dynamic Smagorinsky model. Furthermore, results in the TLES with regularization and RSFS stress are analogous to those in spatial LES and the dynamic mixed model and results in the TLES with only RSFS stress are analogous to those in spatial LES with the scale similarity approximation. In terms of $\bar{u}_2^{\text{rms}}$, the peak value obtained in TLES with regularization and RSFS stress slightly under-predicts the DNS value, a desirable result. The peak value in TLES with only regularization is slightly higher. In terms of $\bar{u}_3^{\text{rms}}$, both, TLES with regularization and RSFS stress and TLES with only regularization, under-predict the peak DNS values, again a desirable feature. Overall, in terms of both $\bar{u}_2^{\text{rms}}$ and $\bar{u}_3^{\text{rms}}$, results of TLES are analogous to those of spatial LES in the same fashion as described earlier.

Although the TLES with only RSFS stress under-predicts the DNS peak value of $\bar{u}_1^{\text{rms}}$, it predicts greater near-wall values of $\bar{u}_2^{\text{rms}}$ and $\bar{u}_3^{\text{rms}}$ than the other two variations of TLES. This characteristic along with its effective over-prediction of 1–3 Reynolds shear stress and severe under-prediction of mean velocity, suggest that TLES with only RSFS stress lacks sufficient turbulent kinetic energy (TKE) dissipation. Such a characteristic of TLES with only RSFS stress is similar to that of spatial LES with the scale similarity approximation, In the dynamic mixed model, in which the scale similarity approximation is used in conjunction with the dynamic Smagorinsky model, the former is known to have a relatively small contribution to TKE dissipation. In fact, in the near wall region, the scale similarity portion of the dynamic mixed model behaves as a source of TKE instead of a sink, as shown in Morinishi and Vasilyev (2001).

In Fig. 8, we plot dissipation due to regularization and RSFS stress in our three variations of TLES. Dissipation due to the RSFS stress dissipation that appears in the transport equation of filter scale turbulent kinetic energy,

$$\bar{k} = \frac{1}{2}(\langle \bar{u}_i \bar{u}_i \rangle - \langle \bar{u}_i \rangle \langle \bar{u}_i \rangle) \tag{18}$$

is defined by

$$\epsilon_{\text{RSFS}} = -\langle \tau_{ij}^{\text{RSFS}} \overline{S}_{ij} \rangle + \langle \tau_{ij}^{\text{RSFS}} \rangle \langle \overline{S}_{ij} \rangle. \tag{19}$$

The dissipation due to regularization is given by

$$\epsilon_{\text{Reg}} = -\chi_1 \langle (\bar{u}_i - \bar{v}_i)\bar{u}_i \rangle + \chi_1 \langle \bar{u}_i - \bar{v}_i \rangle \langle \bar{u}_i \rangle. \tag{20}$$

In TLES with only RSFS stress, TKE dissipation due to RSFS stress increases rapidly moving away from the wall, but then suddenly decreases with further distance from the wall, eventually becoming negative. In the core region of the channel, this dissipation becomes positive, but is very small. A similar behavior is seen in the TKE dissipation

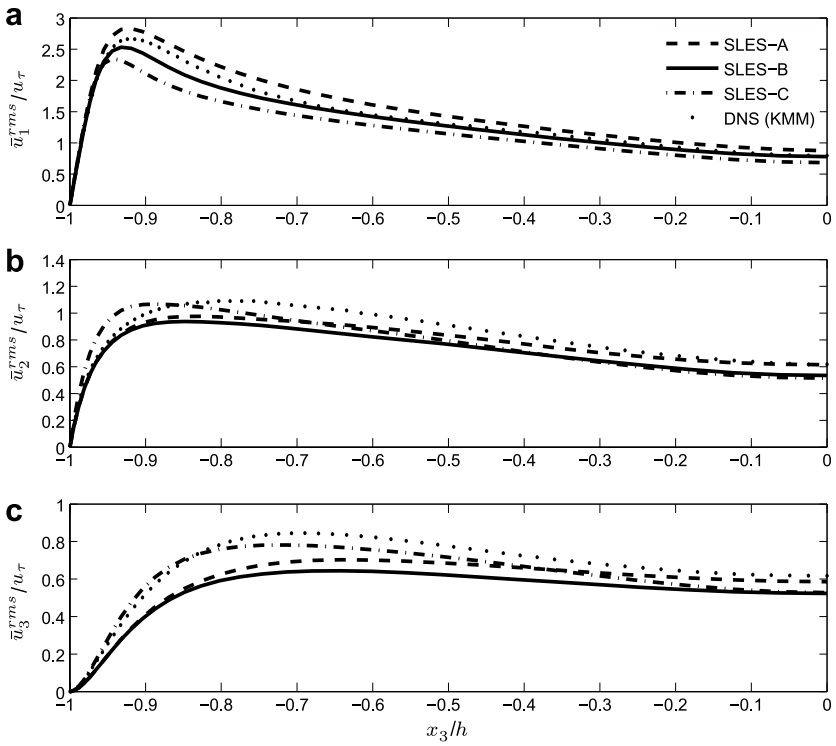

Fig. 7. Root mean square of resolved velocity fluctuations in spatial LES of unstratified flows. SLES-A: spatial LES with dynamic Smagorinsky model; SLES-B: spatial LES with dynamic mixed model; SLES-C: spatial LES with scale similarity approximation; DNS (KMM): direct numerical simulation of Kim, Moin and Moser in Kim et al. (1987).

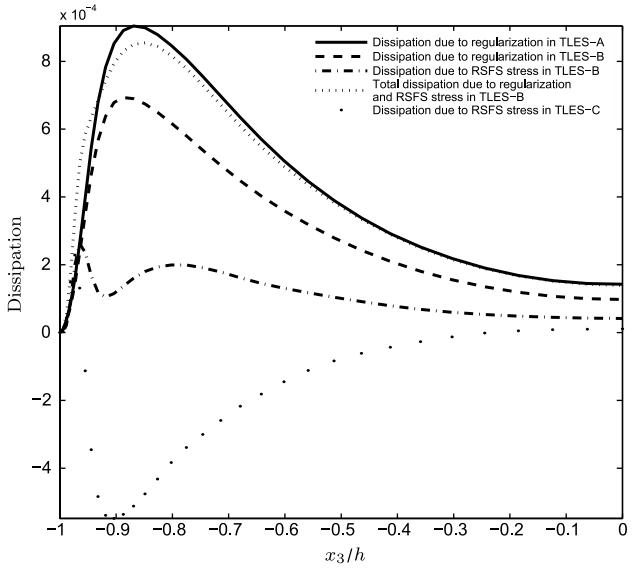

Fig. 8. Resolved TKE dissipation due to regularization and RSFS stress in TLES of unstratified flows. TLES-A: TLES with regularization of momentum only; TLES-B: TLES with both regularization of momentum and RSFS stress; TLES-C: TLES with RSFS stress only.

due to the scale similarity approximation in a spatial LES with only the scale similarity stress, shown in Morinishi and Vasilyev (2001).

In TLES with regularization and RSFS stress, TKE dissipation due to RSFS stress behaves differently compared to its counterpart in TLES with only RSFS stress, as it remains positive (although small) throughout the entire channel. In TLES with regularization and RSFS stress, TKE dissipation due to regularization is less than its counterpart in TLES with only regularization. This suggests that regularization in the former case senses the presence of the RSFS stress serving to dissipate TKE. Remarkably, although regularization and RSFS stress contribute to TKE dissipation in TLES with both, the subfilter-scale TKE dissipation (i.e. total dissipation due to regularization and RSFS stress) is not higher than the dissipation due to regularization in TLES with only regularization.

5. Stably stratified turbulent channel flow

We present results from our extension of TLES to stably, thermally stratified turbulent channel flow at $Re_\tau = 180$ and $Ri_\tau = 60$. We also present results of passive scalar transport in the flow at $Ri_\tau = 0$. In the flow at $Ri_\tau = 60$, stable stratification serves to suppress turbulence intensities near the core or middle of the channel. In terms of perturbation density, $\bar{\rho}$, stable stratification gives rise to a quasi-periodic structure in the core of the channel associated with internal waves (seen in Fig. 9a) co-existing with sustained, wall-generated turbulence in the upper and lower halves. The wall-generated turbulence tends to homogenize $\bar{\rho}$ in the upper and lower halves, away from the middle of the channel. Numerous interesting differences occur between the unstratified and stratified problems, as can be seen in Fig. 9 and other quantities not shown.

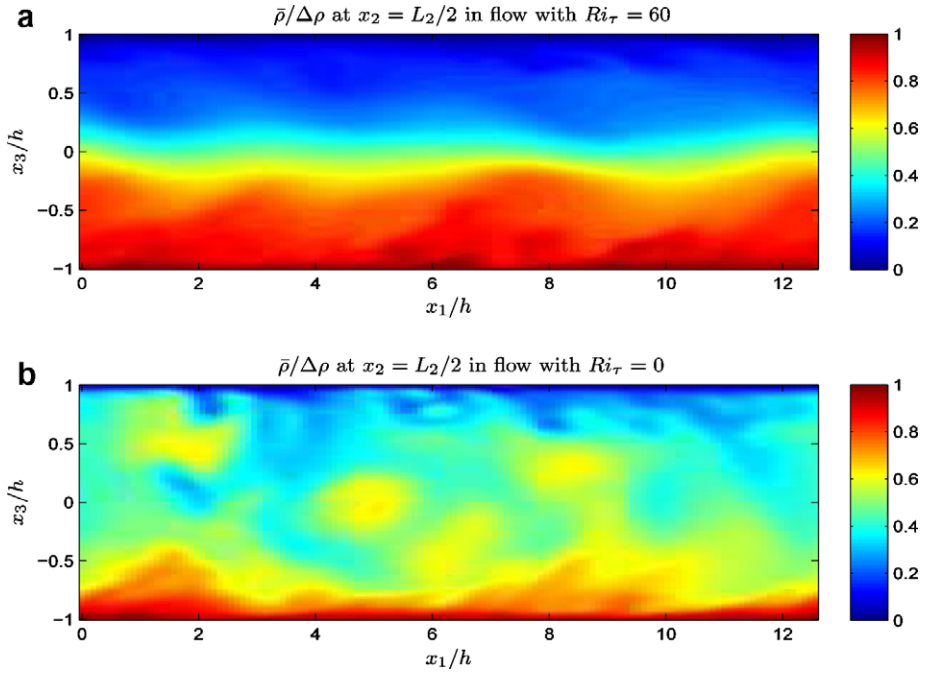

Fig. 9. Instantaneous color plot of resolved perturbation density on an (x_1, x_3)-plane. Results are from TLES with regularization and RSFS stress in the momentum equations and with regularization and RSFS density flux in the scalar transport equation.

The reader is directed to (Armenio and Sarkar, 2002) to learn more about these differences. In our discussion we will point out some of these differences while focusing on the performance of TLES and its comparison to spatial LES and a DNS. Additionally, we will focus on the effect of regularization and RSFS density flux on passive ($Ri_\tau = 0$) and active ($Ri_\tau = 60$) scalar transport. The TLES and the spatial LES presented were performed using the same grid and time step described earlier for LES of unstratified flow. The spatial LES also used the dynamic Smagorinsky model described earlier. Furthermore, in the spatial LES, the SFS density flux was modeled using a dynamic approach (analogous to the dynamic Smagorinsky model) implemented in Armenio and Sarkar (2002). In our case, this dynamic approach involved the same test filter and model parameter described before. The DNS (i.e. with no SFS stress model and no SFS density flux model) was performed with the same $(96 \times 96 \times 97)$ grid and time step described earlier. This was motivated by the success of our previously discussed validation study (see Section 4) in which our DNS of unstratified channel flow at $Re_\tau = 180$ with the $96 \times 96 \times 97$ grid led to results in excellent agreement with the DNS results of Kim et al. (1987).

5.1. Comparison of TLES of passive scalar transport with spatial LES and DNS

Before further discussing results of the stratified flow problem with $Ri_\tau = 60$, we focus on passive scalar statistics in the unstratified ($Ri_\tau = 0$) flow. These results were obtained in TLES with regularization and RSFS stress in the momentum equations and with regularization and RSFS density flux in the scalar transport equation.

An important quantity involving the gradient of mean resolved perturbation density, $\langle\bar{\rho}\rangle$, at the wall is the Nusselt number defined as $Nu = hQ_w/\kappa\Delta\rho$, where $Q_w = (\partial\langle\bar{\rho}\rangle/\partial x_3)_w$ is the density flux at the wall. Note that $(\partial\langle\bar{\rho}\rangle/\partial x_3)_w$ is the averaged vertical gradient of $\langle\bar{\rho}\rangle$ at the top and bottom walls. In the case of purely diffusive mass transport through a stationary fluid, $Nu = 1$. Thus, Nu quantifies the increase of wall mass transport due to turbulence relative to its laminar value. Values predicted by TLES ($Nu = 6.15$) and spatial LES ($Nu = 6.06$) are relatively close to the DNS prediction ($Nu = 6.00$).

Fig. 10a and b show results in terms of mean resolved perturbation density in units of h and in wall units, respectively. In wall units, the mean resolved perturbation density is scaled by $\rho_\tau \equiv Q_w/u_\tau$. In terms of mean perturbation density in units of h, no major differences are observed between the TLES, spatial LES and DNS cases. In terms of mean resolved perturbation density in wall units, a slight difference is observed as the prediction in the TLES compares more favorably with the prediction in the DNS.

Fig. 11a shows results in terms of root mean square of resolved perturbation density fluctuations, $\bar{\rho}^{rms} = \langle\bar{\rho}'^2\rangle^{1/2}$. In the region $|x_3/h| < 0.75$, the TLES prediction is better, and elsewhere the spatial LES prediction is better. Overall, the TLES prediction is comparable to that of spatial LES.

Finally, Fig. 11b shows results in terms of effective resolved density flux. Here TLES outperforms the spatial LES throughout most of the vertical (x_3) extent of the channel. Note that the effective resolved density flux is almost unity away from the wall corresponding to the 'constant flux' hypothesis of neutral boundary layers.

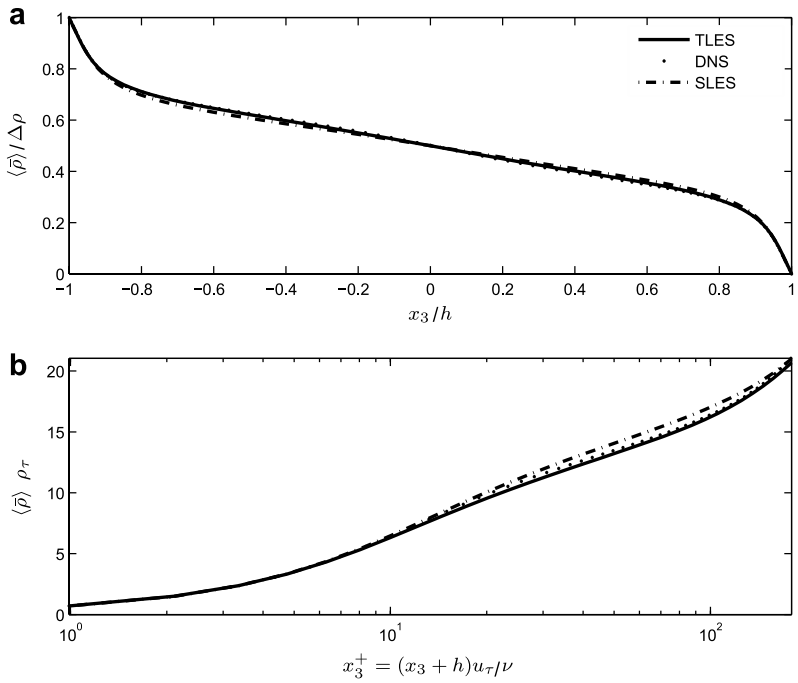

Fig. 10. Mean resolved perturbation density in (a) regular and (b) wall units in unstratified flows ($Ri_\tau = 0$). In TLES, the momentum equations were solved with both regularization and RSFS stress; the scalar transport equation was also solved with regularization and RSFS density flux. Spatial LES (SLES) was performed with dynamic Smagorinsky model and analogous SFS density flux model. Note that the DNS data is nearly indistinguishable from the TLES data.

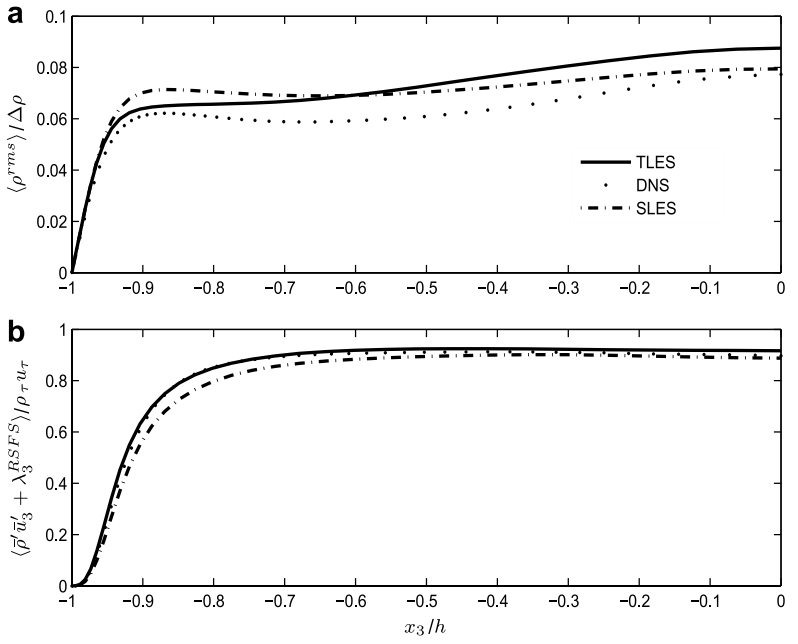

Fig. 11. (a) Root mean square of resolved perturbation density fluctuations and (b) effective resolved density flux in unstratified flows ($Ri_\tau = 0$). In TLES, the momentum equations were solved with both regularization and RSFS stress; the scalar transport equation was also solved with regularization and RSFS density flux. Spatial LES (SLES) was performed with dynamic Smagorinsky model and analogous SFS density flux model. Note that in (b) the DNS data is nearly indistinguishable from the TLES data.

5.2. Effect of regularization and RSFS density flux in TLES of passive scalar transport

Next we study the effects of regularization and RSFS density flux in TLES of passive scalar transport ($Ri_\tau = 0$). In each case presented, the TLES was performed with regularization and RSFS stress in the momentum equations. Three TLES cases are compared to our DNS case. In the first case, a TLES was performed with the scalar transport equation containing regularization only without the RSFS

density flux (TLES-A). In the second case, the scalar transport equation included both regularization and RSFS density flux (TLES-B). A third case was conducted in which the scalar transport equation contained only the RSFS density flux and no regularization (TLES-C).

A summary of the Nusselt numbers, *Nu*, predicted in TLES-A, TLES-B and TLES-C is presented in Table 1. In terms of *Nu*, TLES-A and TLES-B are clearly superior. Furthermore, no significant differences are observed between TLES-A and TLES-B results in terms of mean resolved pertubation density (Fig. 12) and effective resolved density flux (Fig. 13b). Some differences are observed in terms of resolved perturbation density fluctuations, $\bar{\rho}^{\mathrm{rms}} = \langle \bar{\rho}'^2 \rangle^{1/2}$, in Fig. 13b. Here we see that having both RSFS density flux and regularization in the scalar transport equation is clearly better than excluding either one of these two components.

Table 1
Values of *Nu* in TLES, spatial LES (SLES) and DNS of unstratified ($Ri_\tau = 0$) and stratified ($Ri_\tau = 60$) flows

Ri_τ	TLES-A	TLES-B	TLES-C	SLES	DNS
0	6.00	6.15	5.32	6.06	6.00
60	2.29	2.50	2.07	2.69	2.81

In all TLES cases, the momentum equations were solved with regularization and RSFS stress. TLES-A: scalar transport with regularization only; TLES-B: scalar transport with regularization and RSFS density flux; TLES-C: scalar transport with RSFS density flux only. Spatial LES (SLES) was performed with dynamic Smagorinsky model and analogous SFS density flux model.

5.3. Comparison of TLES of active scalar transport with spatial LES and DNS

Next we compare results of TLES of active scalar transport ($Ri_\tau = 60$) with those of spatial LES and DNS. The TLES was carried out with regularization in the momentum equations as well as in the scalar equation for perturbation density, $\bar{\rho}$. Furthermore, the TLES had the RSFS stress in the momentum equations and the RSFS density flux in the scalar transport equation.

Fig. 14 shows results in terms of mean streamwise velocity. Stable stratification suppresses vertical momentum transport relative to unstratified flow leading to a change in the mean velocity in the core region from a flat, well-mixed profile to a curved profile, which would be parabolic in the limit of relaminarization. Looking at Fig. 14a, we see that in the region $20 < x_3^+ < 100$, the mean velocity predicted by TLES is in excellent agreement with that predicted by DNS. In this region, the mean velocity in the spatial LES over-predicts that of the DNS. Both, the TLES and the spatial LES over-predict the velocity in the core region with respect to the DNS.

The suppression of vertical momentum transport by stable stratification is evident in the 1–3 component of the effective resolved Reynolds shear stress, as this quantity is

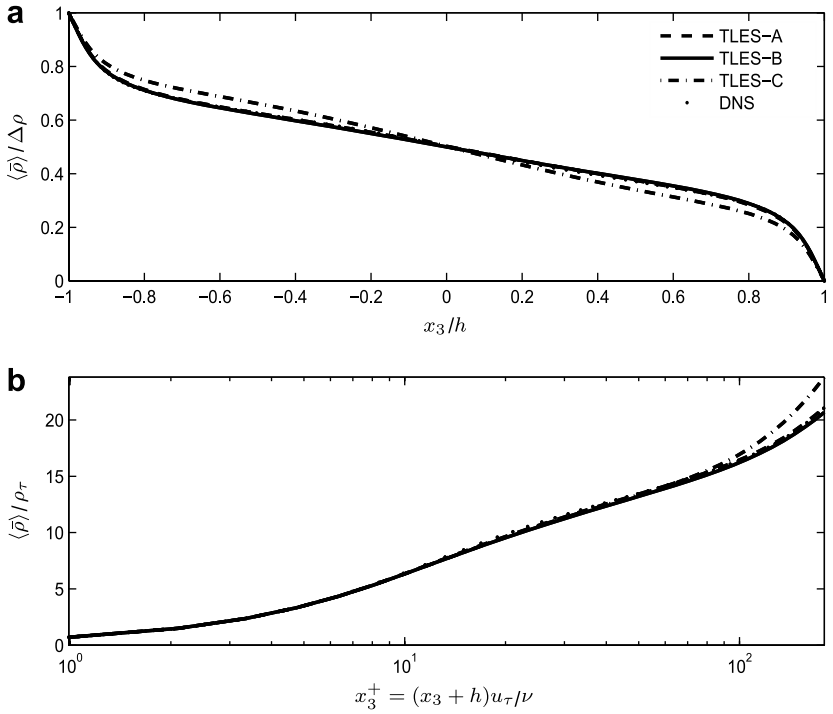

Fig. 12. Mean resolved perturbation density in (a) regular and (b) wall units in TLES of unstratified flows ($Ri_\tau = 0$). In all TLES cases, the momentum equations were solved with regularization and RSFS stress. TLES-A: scalar transport with regularization only; TLES-B: scalar transport with regularization and RSFS density flux; TLES-C: scalar transport with RSFS density flux only. Note that the DNS data, the TLES-A data and the TLES-B data are nearly indistinguishable.

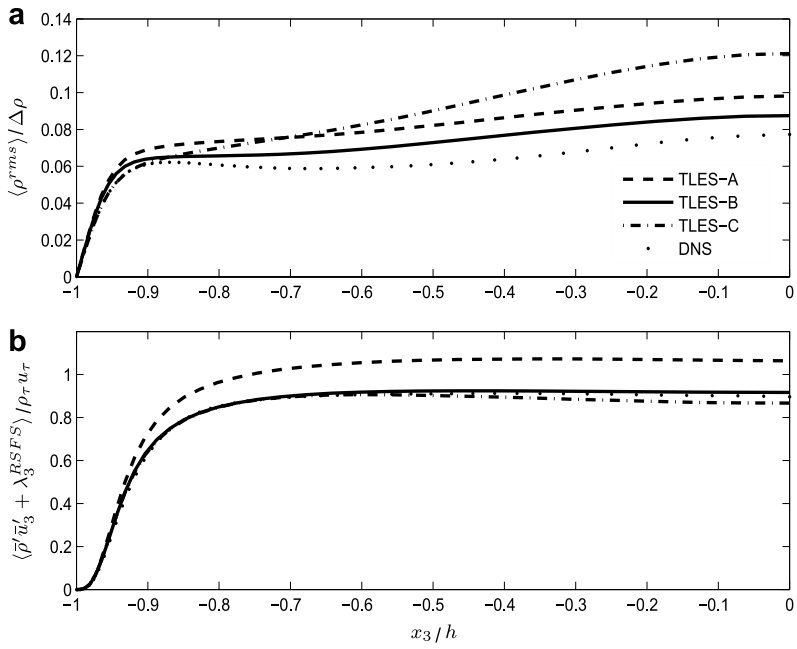

Fig. 13. (a) Root mean square of resolved perturbation density fluctuations and (b) effective resolved density flux in TLES of unstratified flows ($Ri_\tau = 0$). In all TLES cases, the momentum equations were solved with regularization and RSFS stress. TLES-A: scalar transport with regularization only; TLES-B: scalar transport with regularization and RSFS density flux; TLES-C: scalar transport with RSFS density flux only. Note that in (b) the DNS data is nearly indistinguishable from the TLES-B data.

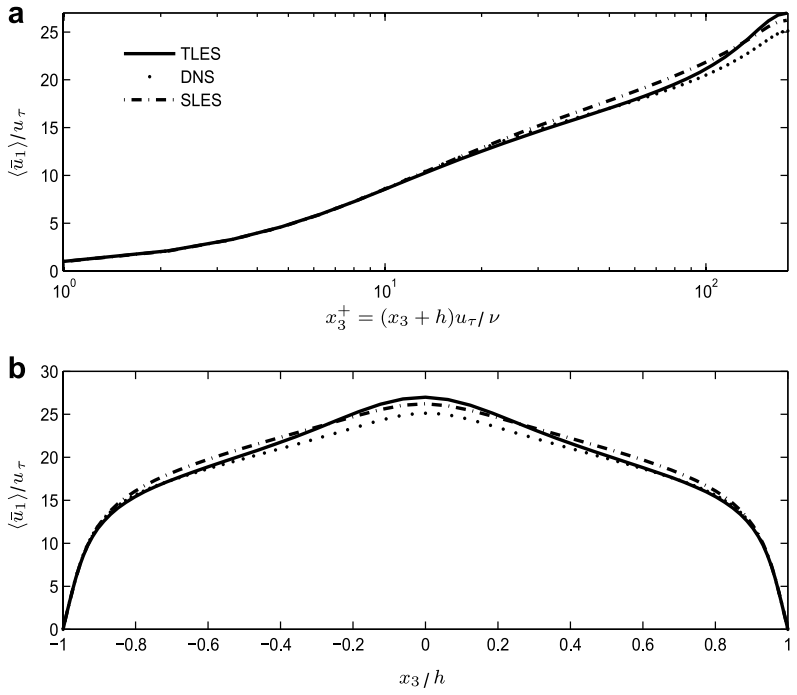

Fig. 14. Mean resolved streamwise velocity in (a) wall units and (b) units of h in stratified flows ($Ri_\tau = 60$). In TLES, the momentum equations were solved with both regularization and RSFS stress; the scalar transport equation was also solved with regularization and RSFS density flux. Spatial LES (SLES) was performed with dynamic Smagorinsky model and analogous SFS density flux model.

lower, especially in the core region of the channel, relative to that in the unstratified flow. This can be seen by comparing the solid curves in Figs. 4 and 15. Furthermore, in Fig. 15 we see that based on effective resolved Reynolds shear stress, the TLES does slightly better than the spatial LES at predicting the peak Reynolds shear stress of the DNS.

Fig. 16 shows root mean square of resolved velocity fluctuations, $\bar{u}_i^{\mathrm{rms}}$, in our stratified flows. In terms of $\bar{u}_1^{\mathrm{rms}}$, both, the TLES and the spatial LES over-predict the peak value

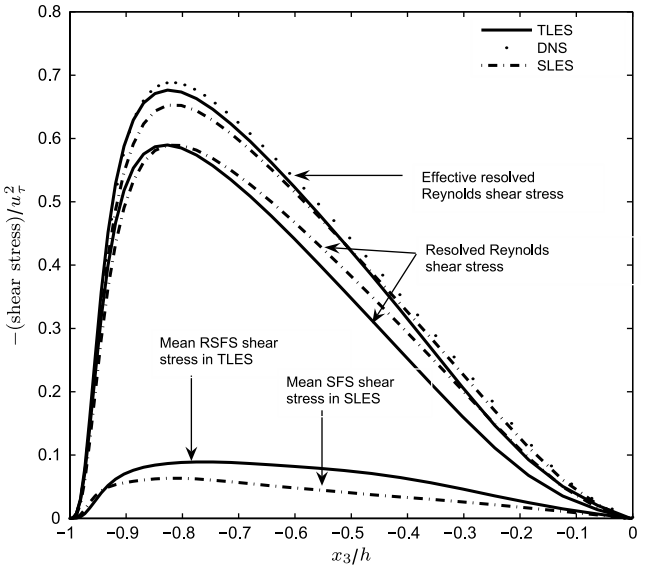

Fig. 15. One to three components of resolved Reynolds shear stress, effective resolved Reynolds shear stress and mean RSFS shear stress or mean SFS shear stress in stratified flows ($Ri_\tau = 60$). In TLES, the momentum equations were solved with both regularization and RSFS stress; the scalar transport equation was also solved with regularization and RSFS density flux. Spatial LES (SLES) was performed with dynamic Smagorinsky model and analogous SFS density flux model.

of the DNS. Conversely, in terms of $\bar{u}_2^{\text{rms}}$ and $\bar{u}_3^{\text{rms}}$, the TLES and the spatial LES under-predict the peak value of the DNS. This latter result is desirable given that the DNS velocity field has not been filtered.

In terms of the Nusselt number, Nu, TLES yields $Nu = 2.50$, the spatial LES yields $Nu = 2.69$ and the DNS yields $Nu = 2.81$. The spatial LES of Armenio and Sarkar (2002) predicted $Nu = 2.79$. Note that in the LES of Armenio and Sarkar (2002), the grid was $(48 \times 64 \times 64)$, and recall that in our DNS, the grid was $(96 \times 96 \times 97)$, while in our TLES and spatial LES, the grids were $(32 \times 32 \times 65)$. Although the TLES under-predicts the Nu of the DNS, better agreement could potentially be obtained by finding an optimal value of χ_2, the constant coefficient in the regularization term of the scalar equation for $\bar{\rho}$.

The stabilizing effect of stratification is linked to the reduced values of Nu in the stratified flows relative to those in the unstratified flows (see for example Table 1). From the definition of Nu given earlier, this reduction clearly signifies inhibited density at the wall as well as a decrease of mean resolved perturbation density gradient at the wall in the stratified flows relative to the unstratified flows.

Fig. 17a and b show mean resolved perturbation density in units of h and in wall units, respectively. In wall units, the mean resolved perturbation density is scaled by $\rho_\tau \equiv Q_w/u_\tau$. Expressed in units of h, no major differences are visible between the profiles of $\langle\bar{\rho}\rangle$ in TLES, spatial LES and DNS. However, there are differences specially at the walls as the Nusselt numbers (related to the density gradient at the walls) predicted by the three simulations are

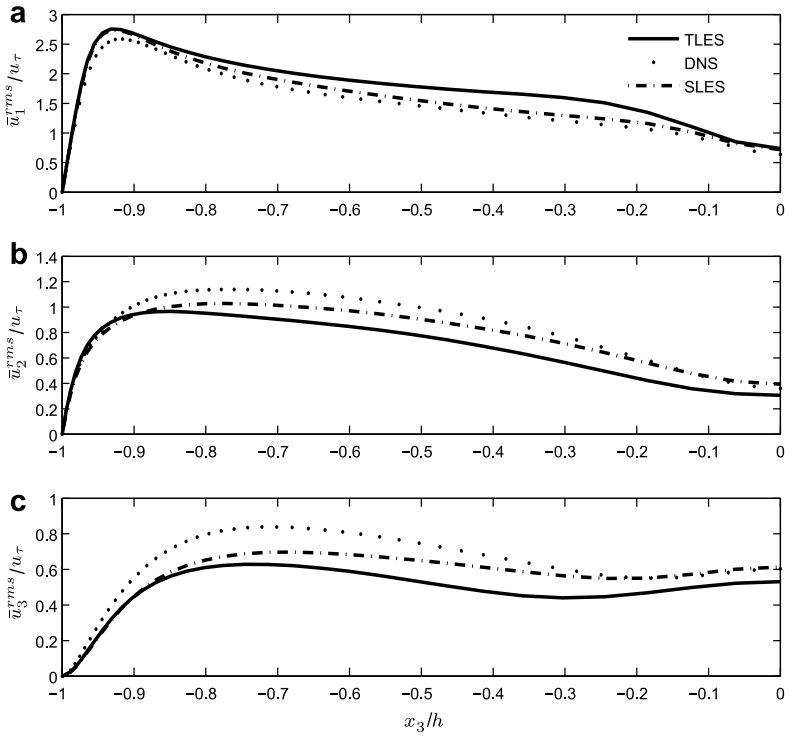

Fig. 16. Root mean square of resolved velocity fluctuations in stratified flows ($Ri_\tau = 60$). In TLES, the momentum equations were solved with both regularization and RSFS stress; the scalar transport equation was also solved with regularization and RSFS density flux. Spatial LES (SLES) was performed with dynamic Smagorinsky model and analogous SFS density flux model.

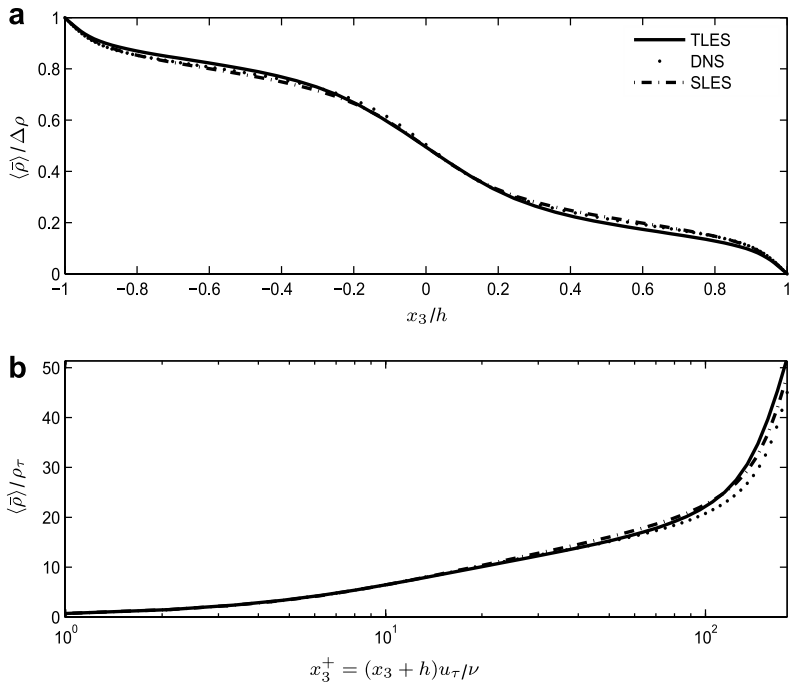

Fig. 17. Mean resolved perturbation density in (a) regular and (b) wall units in stratified flows ($Ri_\tau = 60$). In TLES, the momentum equations were solved with both regularization and RSFS stress; the scalar transport equation was also solved with regularization and RSFS density flux. Spatial LES (SLES) was performed with dynamic Smagorinsky model and analogous SFS density flux model.

different. In terms of wall units, some differences can be seen, especially in the core region of the channel (i.e. for $x_3^+ > 100$). These differences are primarily due to the different predictions of ρ_τ by the three simulations.

It is noteworthy to point out the differences between the mean resolved perturbation density profiles in the stratified flows (Fig. 17a) versus those in the unstratified flows (Fig. 10a). In particular, the non-zero Richardson number

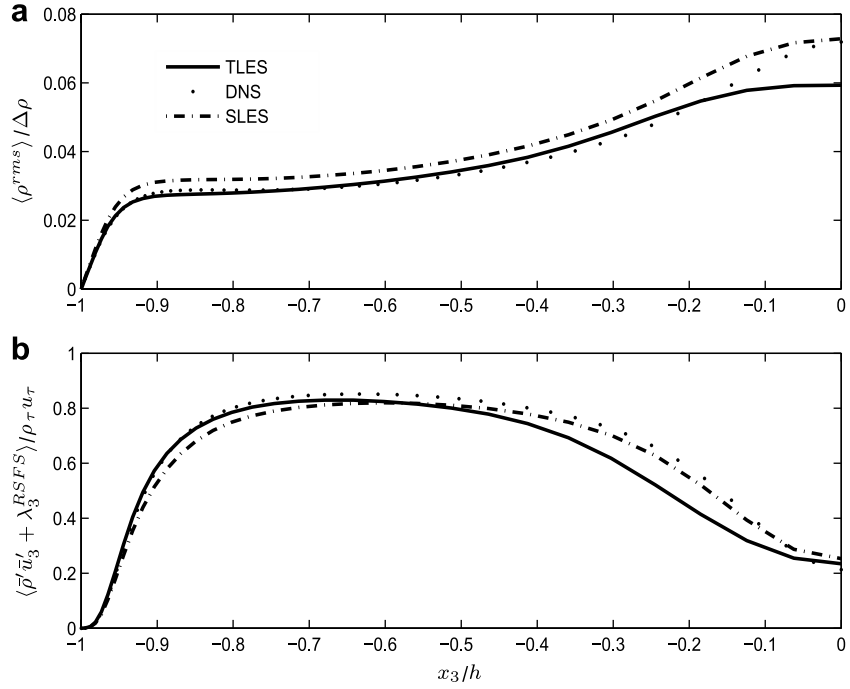

Fig. 18. (a) Root mean square of resolved perturbation density fluctuations and (b) effective resolved density flux in stratified flows ($Ri_\tau = 60$). In TLES, the momentum equations were solved with both regularization and RSFS stress; the scalar transport equation was also solved with regularization and RSFS density flux. Spatial LES (SLES) was performed with dynamic Smagorinsky model and analogous SFS density flux model.

($Ri_\tau = 60$) introduces two main changes with respect to the passive scalar case ($Ri_\tau = 0$). First it reduces the density gradient at the wall, as mentioned earlier. Second, the density profiles become sharper in the core region of the channel revealing a tendency towards a density interface, as was seen in Fig. 9.

Fig. 18a shows root mean square of resolved perturbation density fluctuations, $\bar{\rho}^{\mathrm{rms}} = \langle \bar{\rho}'^2 \rangle^{1/2}$. Given that the DNS is not filtered, it would be desirable for the LES-predicted values to be less than those of the DNS. Away from the core region of the channel (i.e. for $x_3/h < -0.2$) the TLES prediction is very close to the DNS prediction and lower than the spatial LES prediction. In the core region, although the TLES prediction is lower than the DNS prediction, the profile is certainly flatter. In the spatial LES case, the profile is not as flat and its shape is closer to that of the DNS profile. This discrepancy points to different behaviors of the TLES and the spatial LES in the presence of the quasi-periodic structure associated with internal waves (described earlier) in the core region of the channel.

Finally, Fig. 18b shows results of effective resolved vertical density flux in TLES and in spatial LES. The suppression of resolved vertical density flux by stable stratification is evident in the middle or core region of the channel relative to its levels in the upper and lower halves of the channel. This behavior is clearly representative of a supressed turbulent state in the core region co-existing with a more intense, wall-generated turbulent state in the upper and lower halves.

Throughout the channel, both TLES and spatial LES values of effective resolved density flux under-predict those of the DNS. Better agreement with the DNS could, perhaps, be obtained by fine tuning χ_2 in the TLES.

5.4. Effect of regularization and RSFS density flux in TLES of active scalar transport

Next we study the effects of regularization and RSFS density flux in TLES of active scalar transport. In each case presented, the TLES was performed with regularization and RSFS stress in the momentum equations. Three TLES cases are compared to our DNS case. In TLES-A, the scalar transport equation contained regularization only and no RSFS density flux. In TLES-B, the scalar transport equation included both regularization and RSFS density flux. In TLES-C, the scalar transport equation contained only the RSFS density flux and no regularization (TLES-C).

A summary of the Nusselt numbers, *Nu*, predicted in TLES-A, TLES-B and TLES-C is presented in Table 1. Including both regularization and RSFS density flux in the scalar transport equation is beneficial as TLES-B predicts a better value of *Nu* than TLES-A and TLES-C. This same conclusion can be made in terms of mean resolved perturbation density (Fig. 19) and effective resolved density flux (Fig. 10b). For example, in terms of the latter, in the core region of the channel ($|x_3/h| < 0.6$), TLES-B and TLES-C predictions are nearly identical and in good agreement with the DNS prediction, while the TLES-A prediction is much worse. The situation is reversed in the core region of the channel as the TLES-B and TLES-A predictions are close to each other and in good agreement with

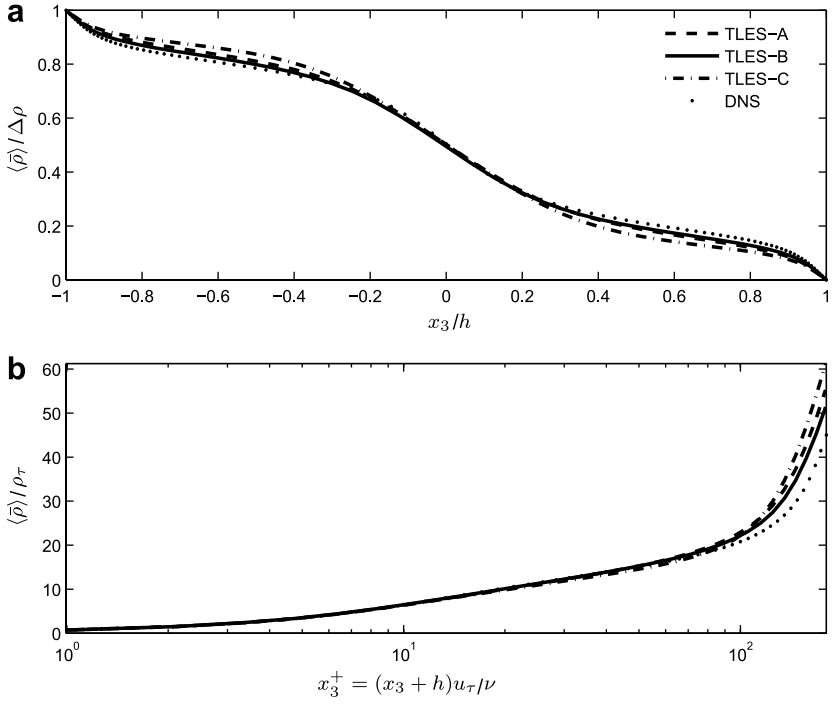

Fig. 19. Mean resolved perturbation density in (a) regular and (b) wall units in TLES of stratified flows ($Ri_\tau = 60$). In all TLES cases, the momentum equations were solved with regularization and RSFS stress. TLES-A: scalar transport with regularization only; TLES-B: scalar transport with regularization and RSFS density flux; TLES-C: scalar transport with RSFS density flux only.

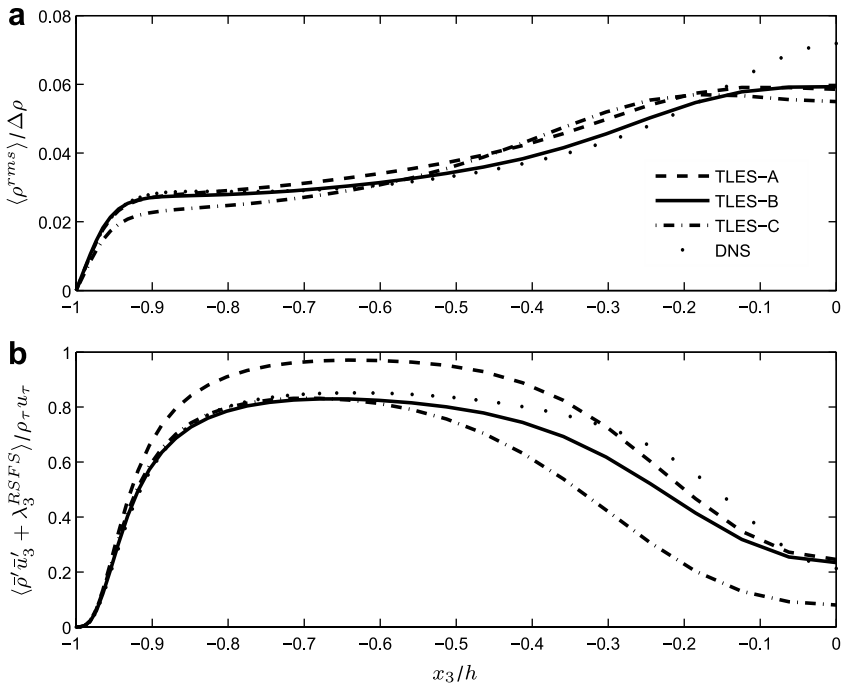

Fig. 20. (a) Root mean square of resolved perturbation density fluctuations and (b) effective resolved density flux in TLES of stratified flows ($Ri_\tau = 60$). In all TLES cases, the momentum equations were solved with regularization and RSFS stress. TLES-A: scalar transport with regularization only; TLES-B: scalar transport with regularization and RSFS density flux; TLES-C: scalar transport with RSFS density flux only.

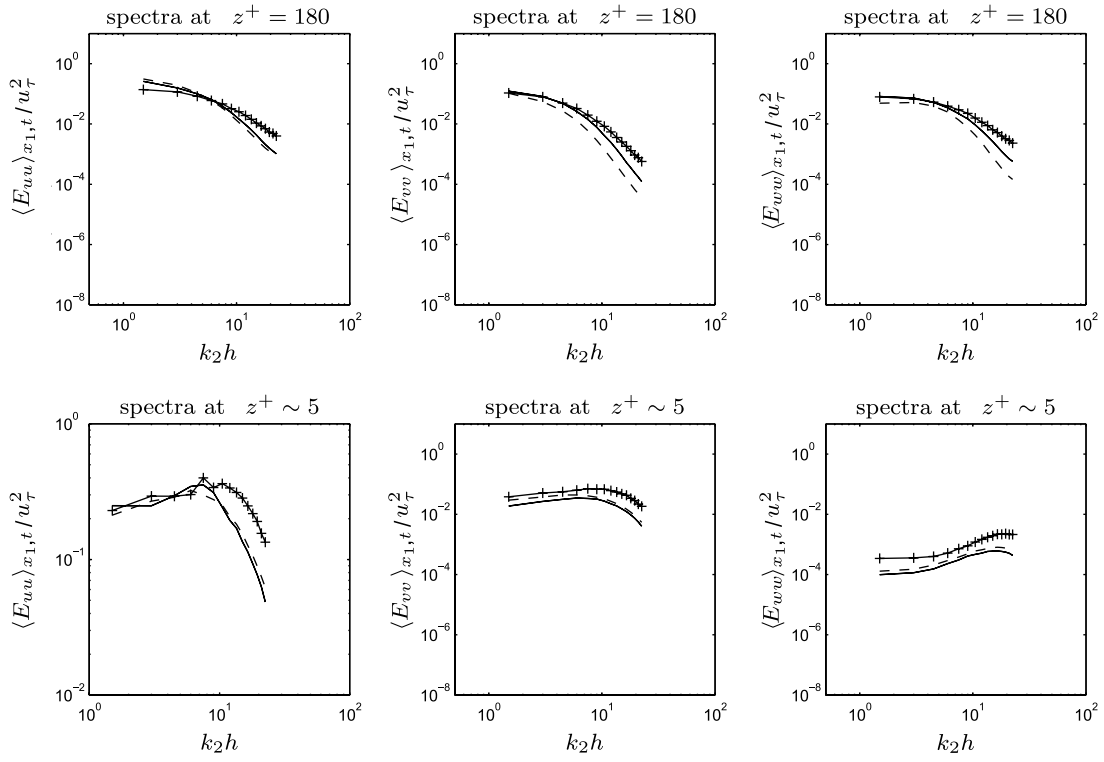

Fig. 21. One-dimensional spanwise energy spectra in the middle ($z^+ = 180$) and in the near-wall ($z^+ \sim 5$) regions of unstratified turbulent channel flow. E_{uu}: spectra based on autocorrelation of streamwise velocity component. E_{vv}: spectra based on autocorrelation of spanwise velocity component. E_{ww}: spectra based on autocorrelation of wall-normal velocity component. k_2 denotes the dimensionless spanwise wavenumber and $\langle \cdot \rangle_{x_1,t}$ denotes averaging in time and over the streamwise direction. Solid: spectrum obtained in dynamic model spatial LES; plus, +: spectrum obtained in simulation with no SFS stress nor regularization; dashed: spectrum obtained in TLES with regularization and RSFS stress.

the DNS prediction, while the TLES-C prediction is much worse. No such appreciable differences are observed in terms of resolved perturbation density fluctuations, $\bar{\rho}^{\mathrm{rms}}$ (see Fig. 20).

6. Concluding remarks

The effects of regularization and RSFS stress in TLES of unstratified turbulent channel flow at $Re_\tau = 180$ were clarified. Overall, TLES with only regularization and TLES with both regularization and RSFS stress led to similar results. Given this observation, it would seem plausible to retain the former in future simulations. However, the latter possesses the merit that the RSFS stress is strongly correlated with the exact SFS stress, as demonstrated in Pruett et al. (2003) for Burgers equation. Furthermore, the RSFS stress may potentially account for backscatter in more complex flows. Thus, we interpret TLES with regularization and RSFS stress as analogous to the well-known dynamic mixed model in spatial LES. Similar to the Smagorinsky portion of the dynamic mixed model, regularization can provide sufficient turbulent kinetic energy dissipation. Similar to the scale similarity portion of the dynamic mixed model, the RSFS stress can provide higher correlation with the exact SFS stress. We note that our conclusions regarding the effects of the RSFS stress and regularization may not be applicable to channel flows at higher Reynolds number and future efforts will be made to hopefully show that this is not the case. Future research will also concentrate on a more physics-based alternative to modeling the USFS stress instead of the artificial, purely dissipative type mechanism provided by regularization.

Finally, we have shown that TLES performs on par with spatial LES with the dynamic Smagorinsky model on stably stratified turbulent channel flow ($Re_\tau = 180, Ri_\tau = 60$) as it is able to properly capture the suppression of turbulence in the core of the channel co-existing with higher levels of wall-generated turbulence in the upper and lower halves. We conjecture that improvements could be made via proper tuning of the regularization parameter χ_2 appearing in the scalar transport equation. For the cases of passive ($Ri_\tau = 0$) and active ($Ri_\tau = 60$) scalar transport, it was shown that including both regularization and RSFS density flux in the scalar transport equation is beneficial for predictions such as the Nusselt number and the effective resolved density flux.

As noted in Section 1, TLES relies on the premise that the removal of high-frequency content from the frequency spectrum should effectively remove high-wavenumber content from the wavenumber spectrum as well. In an initial attempt to confirm this, we ran three cases of the unstratified turbulent channel flow for which we computed one-dimensional, streamwise and spanwise energy spectra. The first case is a spatial LES with the dynamic Smagorinsky model, the second case is a TLES with RSFS stress and regularization, and the third case is a simulation with no SFS stress model nor regularization (i.e. a no-model case). All cases were performed on the $(32 \times 32 \times 65)$ grid. Fig. 21 shows spanwise spectra based on autocorrelation of the different velocity components for the three cases. In the TLES and spatial LES cases, spectra at the highest wave numbers is more attenuated than spectra in the no-model case. In the middle of the channel, the spanwise spectra based on spanwise and wall-normal velocity autocorrelations are more attenuated for the TLES case than for the spatial LES case. In the near-wall region, spectra in the TLES and spatial LES cases are very similar. These results clearly indicate that there is a spatial filter associated with TLES which is at least as dissipative as the spatial filter in dynamic model LES, thus supporting the statement of Pruett et al. (2006) suggesting that removal of high-frequency content effectively removes high-wave number content.

Future work will go towards further deciphering the spatial filtering induced in TLES. Future research will also explore extensions of TLES to unstructured grid methods. In the case of finite volume methods, we would first have to explore the implications of applying the time filter together with the spatial average used to derive the governing equations.

Acknowledgement

A.E.T.-M. and C.E.G. acknowledge the support of the NASA Langley Research Center through Grant No. NNL05AA10G.

References

Armenio, V., Sarkar, S., 2002. An investigation of stably stratified turbulent channel flow using large-eddy simulation. J. Fluid Mech. 459, 1–42.

Armfield, S.W., Street, R.L., 2000. Fractional step methods for the Navier–Stokes equations on non-staggered grids. ANZIAM J. 42 (E), C134–C156.

Bardina, J., Ferziger, J.H., Reynolds, W.C., 1983. Improved turbulence models based on large eddy simulation of homogeneous, incompressible, turbulent flows. Stanford University Tech. Rep. TF-19.

Fringer, O.B., Armfield, S.W., Street, R.L., 2003. A nonstaggered curvilinear grid pressure correction method applied to interfacial waves. In: Proceedings of the 2nd International Conference on Heat Transfer, Fluid Mechanics, and Thermodynamics, Paper number FO1.

Gullbrand, J., Chow, F.K., 2003. The effect of numerical errors and turbulence models in large-eddy simulation of channel flow, with and without explicit filtering. J. Fluid Mech. 495, 323–341.

Horiuti, K., 1989. The role of the Bardina model in large eddy simulation of turbulent channel flow. Phys. Fluids A 1, 426–428.

Kim, K., Moin, P., Moser, R., 1987. Turbulence statistics in fully developed channel flow at low Reynolds number. J. Fluid Mech. 177, 133–166.

Lilly, D.K., 1992. A proposed modification of the Germano subgrid-scale closure. Phys. Fluids 3, 2746–2757.

Lund, T.S., 1997. On the use of discrete filters for large-eddy simulation. In: Annu. Res. Briefs, Center for Turbulence Research, NASA Ames/Stanford University, pp. 83–95.

Morinishi, Y., Vasilyev, O.V., 2001. A recommended modification to the dynamic two-parameter mixed subgrid scale model for large eddy simulation of turbulent flows. Phys. Fluids 13, 3400–3410.

Pope, S.B., 2000. Turbulent Flows. Cambridge University Press.

Pruett, C.D., Gatski, T.B., Grosch, C.E., Thacker, W.D., 2003. The temporally filtered Navier–Stokes equations: properties of the residual stress. Phys. Fluids 15, 2127–2140.

Pruett, C.D., Thomas, B.C., Grosch, C.E., Gatski, T.B., 2006. A temporal approximate deconvolution model for LES. Phys. Fluids 18, 028104, 4 p.

Salvetti, M.V., Banerjee, S., 1994. A priori tests of a new dynamic subgrid-scale model for finite-difference large-eddy simulations. Phys. Fluids 7, 2831–2847.

Stolz, S., Adams, N.A., 1999. An approximate deconvolution procedure for large-eddy simulation. Phys. Fluids 11, 1699–1701.

Tejada-Martínez, A.E., Grosch, C.E., 2006. Langmuir turbulence in shallow water. Part 2. Large-eddy simulation. J. Fluid Mech. 576, 63–108.

Yong, Z., Brasseur, J.G., Anurag, J., 2001. A resolvable subfilter-scale model specific to large-eddy simulation of under-resolved turbulence. Phys. Fluids 13, 2602–2610.

Zang, Y., Street, R.L., Koseff, J.R., 1993. A dynamic subgrid-scale model and its application to turbulent recirculating flows. Phys. Fluids A 5, 3186–3196.